Punching Capacity of Prestressed Concrete Bridge Decks Under Fatigue

Lantsoght, Eva; van der Veen, Cor; Koekkoek, Rutger; Sliedrecht, Henk

DOI
10.14359/51715563

Publication date
2019

Document Version
Accepted author manuscript

Published in
ACI Structural Journal

Citation (APA)
Lantsoght, E., van der Veen, C., Koekkoek, R., & Sliedrecht, H. (2019). Punching Capacity of Prestressed Concrete Bridge Decks Under Fatigue. *ACI Structural Journal*, *116*(4), 209-218. https://doi.org/10.14359/51715563

PUNCHING CAPACITY OF PRESTRESSED CONCRETE BRIDGE DECKS UNDER FATIGUE

Eva O. L. Lantsoght[1,2,3], Cor van der Veen[1], Rutger Koekkoek[4], and Henk Sliedrecht[5]

[1] Concrete Structures, Delft University of Technology, Delft, The Netherlands

[2] Universidad San Francisco de Quito, Quito, Ecuador

[3] Adstren, Quito, Ecuador

[4] BAM Infraconsult, Gouda, the Netherlands

[5] Rijkswaterstaat, Ministry of Infrastructure and the Environment, Utrecht, the Netherlands

Biography: ACI member **Eva Lantsoght** is a full professor at Universidad San Francisco de Quito, a researcher at Delft University of Technology, The Netherlands, and a structural engineer at Adstren, Ecuador. She is a member of ACI 445-0D Shear Databases, ACI-ASCE 421 Design of Reinforced Concrete Slabs, ACI 342 Evaluation of Concrete Bridges and Bridge Elements, and an associate member of ACI 437 Strength Evaluation of Existing Concrete Structures, and ACI-ASCE 445 Shear and Torsion.

Cor van der Veen is an associate professor at Delft University of Technology, Delft, The Netherlands. He received his MSc and PhD from Delft University of Technology. He is a member of various National Committees. His research interests include (very) high strength (steel fiber) concrete, concrete bridges and computational mechanics.

Rutger Koekkoek is a maritime engineer at BAM Infraconsult. Formerly he was a researcher at Delft University of Technology where he prepared and executed several outdoor load tests and did fatigue tests on transversally precast bridge decks and shear tests on prestressed beams.

Henk Sliedrecht is a senior consultant at Rijkswaterstaat, Ministry of Infrastructure and Watermanagement, Utrecht, The Netherlands. He received his MSc from Delft University of Technology. His research interests include the assessment of existing concrete bridges in particular methods of analysis and standards for structural safety.

ABSTRACT

Previous research showed that the capacity of existing slab-between-girder bridges is larger than expected based on the punching shear capacity prescribed by the governing codes, as a result of compressive membrane action. A first series of fatigue tests confirmed that compressive membrane action also acts under cycles of loading. However, a single experiment in which first a number of cycles with a higher load level and then with a lower load level were applied, seemed to indicate that this loading sequence shortens the fatigue life. This topic was further investigated in a second series of fatigue tests with three static tests and ten fatigue tests. The parameters that were varied are the sequence of loading and the effect of a single or a double wheel print. The results show that the sequence of load levels does not influence the fatigue life.

Keywords: bridge evaluation; compressive membrane action; concrete bridges; fatigue; fatigue testing; laboratory testing; prestressed concrete; punching shear.

INTRODUCTION

In the Netherlands, a large number of existing bridges require assessment (Lantsoght et al., 2013a). Certain bridge types typically do not fulfil the current code requirements. For example, the shear capacity of reinforced concrete slab bridges is often found to be insufficient (Lantsoght et al., 2013b). Similarly, the punching shear capacity according to NEN-EN 1992-1-1:2005 (CEN, 2005) of the slabs in slab-between-girder bridges is often found to be insufficient under the NEN-EN 1991-2:2003 (CEN, 2003) loads. In total, about 70 slab-between-girder bridges in the Netherlands need to be assessed (Koekkoek et al., 2018).

The punching shear capacity expression from NEN-EN 1992-1-1:2005 (CEN, 2005) is an empirical expression that is derived from experiments on slab-column connections (Regan and Braestrup, 1985; Walraven, 2002). These specimens mimic the behavior of slab-column connections in reinforced concrete buildings up to the point of contraflexure in the slab. Most specimens have a small depth and are heavily reinforced to make sure the failure mode in the slab is punching instead of flexure. For punching of bridge decks cast in between concrete girders and subjected to concentrated loads resulting from traffic, the load-carrying behavior differs significantly from slab-column connections. In the slab-between-girder bridges, the short length of the slabs between the prestressed girders results in the activation of compressive membrane action. This effect enhances the load-carrying capacity of the structure.

To incorporate the enhancement from compressive membrane action in the assessment of slab-between-girder bridges, the static and fatigue strength need to be evaluated. A first part of this research program focused on the static strength and the mechanics of compressive membrane action in thin transversely prestressed concrete decks (Amir, 2014; Amir et al., 2016). On the same test setup, exploratory fatigue tests raised concerns with regard to the activation of compressive membrane action under fatigue loading. Therefore, a new deck was cast as part of the original test setup, and a first series of fatigue tests was carried out (Lantsoght et al., in review). These results

indicated that compressive membrane action still enhances the punching capacity of slab-between-girder bridges under fatigue loading, but that two parameters needed further study: the effect of the sequence of load level in variable amplitude fatigue tests, requiring the confirmation of the validity of Miner's rule (van Leeuwen and Siemes, 1979) for the studied bridge system, and the effect of a single wheel load versus double wheel loads.

This paper presents the results of a second series of experiments on a completely new bridge setup, which differs from the setup used in the first series. These experiments were designed to study the sequence of load levels for variable amplitude loading, and to check if the fatigue life for slab-between-girder decks under fatigue loading with a high load level followed by a lower load level is reduced as compared to the case with a lower load level followed by a higher load level.

Experiments on the effect of variable amplitude fatigue loading on structural systems are scarce. For experiments on small copper elements, there is an indication that high-to-low loading levels of variable amplitude loading cannot be represented with Miner's rule, whereas low-to-high loading levels of variable amplitude loading fit Miner's rule (Ghammouri et al., 2011). The validity of these results for concrete structures is questionable. For seismic applications, experimental research found that the effect of variable amplitude loading can be expressed based on damage models (El-Bahy et al., 1999). Constant and variable amplitude fatigue load tests have been used to confirm the performance of concrete bridge deck slabs with glass FRP bars (El-Ragaby et al., 2007) and CFRP bars (Ju et al., 2017). The effect of variable amplitude loading may need to be modelled with nonlinear damage accumulation models (Chen et al., 2018), with their application limited to modelling uniaxial material behavior (Keerthana and Chandra Kishen, 2018). However, given the large scatter on typical fatigue test results of structural systems, such damage accumulation models may not lead to practical results for the validation of the fatigue life of new bridge systems or the study of the fatigue life of existing bridge systems. Therefore, this study will only evaluate if applying the derived Wöhler curve from the first series of experiments is conservative for high-to-

low load levels with variable amplitude fatigue loading.

The discussion with regard to the effect of the sequence of load levels for variable amplitude loading has a direct practical implication. Originally, for the assessment of existing bridges in the Netherlands, it was assumed that the variations on the load magnitude are limited. Weigh-in-motion measurements, however, showed that on an annual basis 10 to 20 extreme axle loads could be registered. These axles had a load of 350 kN (79 kip), which is almost three times larger than the maximum allowed 120 kN (27 kip).

RESEARCH SIGNIFICANCE

The presented experiments are unique since they study behavior at the structural level rather than at the member level. These experiments study the influence of different types of variable amplitude loading on the fatigue life, which is not commonly studied on large structural concrete setups. These experiments, together with the first series of fatigue tests on a half-size slab-between-girder bridge, show that compressive membrane action enhances the ultimate capacity of transversely prestressed bridge decks under static and fatigue loading. These results are valuable for the assessment of existing slab-between-girder bridges.

PREVIOUS FATIGUE TESTING ON TRANSVERSELY PRESTRESSED CONCRETE DECKS

In previous research (Amir, 2014; Amir et al., 2016), the punching capacity of slab-between-girder bridges was studied experimentally in the laboratory on a half-scale specimen modeled after an existing bridge. This same specimen was subjected to four additional static tests, two tests with three cycles per load level, and seven fatigue tests. Five tests were carried out on the original specimen, and eight tests were carried out on a newly cast deck (Lantsoght et al., in review). Punching was the failure mode in all cases.

The test setup contained in total four prefabricated prestressed concrete girders, three transversely prestressed slab decks cast in situ in between the girders, and two cast in situ prestressed transverse beams. The overall dimensions of the test specimen were 12 m (39 ft) × 6.4 m (21 ft). The deck had a thickness of 100 mm (4 in).

Three parameters were studied with these experiments. The influence of the spacing between the prestressing ducts on the ultimate load was found to be small. Variable amplitude loading with a high load level followed by a low load level resulted in a lower fatigue life than for a low load level followed by a high load level. However, only one experiment was used for this observation. Therefore, this parameter was identified as a topic for future research. For the static tests, the maximum load when a double wheel load is used was 1.48 times the maximum load when a single wheel load is used. Only one dynamic test with a double wheel load was done. The results from this test seem to follow the same trend as the results with a single wheel load. The difference between a single and double wheel load was also identified as an interested topic for further study, especially since this loading configuration is more related to practice.

The following *S*-*N* curve (average values) resulted from the experiments of the first series:

$$S = -0.062 \log N + 0.910 \quad (1)$$

From this expression, it follows that at 1 million cycles, the fatigue strength is 54% of the static strength, at 10 million cycles the ratio is 48%, and at 100 million cycles 41%. Similar ratios are observed for concrete under compression and for fatigue tests on structural elements (Lantsoght et al., 2016). As such, the experiments showed that compressive membrane action also acts under fatigue loading.

EXPERIMENTAL INVESTIGATION

Test setup

The test setup is a half-scale representation of an existing slab-between-girder bridge. The main

elements of the setup are three ZIP600 prefabricated prestressed concrete girders, two transversally prestressed deck slabs cast in situ between the girders, and two prestressed transverse beams cast in the laboratory, see **Fig. 1**. The overall dimensions of the setup are 12 m (39 ft) × 4.6 m (15 ft). The main difference with the test setup from the first series is that both the top flange and slabs are cast in the laboratory in these experiments, and that these are cast together resulting in a monolithic deck, whereas for the previous setup only the slabs were cast in between the girders. However, the static tests in the first series (Amir et al., 2016) showed that failure does not occur at the interface between the prefabricated girder and the cast-in-situ slab. This difference is thus expected to be of minor importance.

To build the setup, first the prefabricated girders were delivered and placed on the supports, and for lateral stability, temporary supports were provided (**Fig. 2**a). Then, the crossbeams were cast and prestressed, and the temporary supports of the girders were removed. In a last step, the formwork for the top flanges and deck was made (**Fig. 2**b), the reinforcement was placed in the formwork (**Fig. 2**c), the concrete was cast (**Fig. 2**d), and the transverse prestressing applied. **Fig. 2**e shows an overview of the completed test setup. **Fig. 3** shows the geometry of the cross-section of the prefabricated prestressed girders.

Material properties

The concrete of the crossbeams, deck slab, and top flanges of the girders was cast in the laboratory with concrete delivered by truck mixer. Three batches of concrete were used: one for the crossbeams, and then two at a later date for the deck slab and top flanges. The average cube compressive strength of the concrete of the crossbeams at 149 days was $f_{cm,cube}$ = 78.3 MPa (11,356 ksi) and the average splitting tensile strength at that age was $f_{sp,m}$ = 5.2 MPa (754 psi). The average cube compressive strength of the first cast of the deck and top flanges at 28 days was $f_{cm,cube}$ = 80.6 MPa (11,690 ksi) and $f_{sp,m}$ = 6.1 MPa (885 psi). For cast two, the measured concrete properties at 28 days were $f_{cm,cube}$ = 78.6 MPa (11,400 psi) and $f_{sp,m}$ = 6.4 MPa (928 psi). The measured concrete

compressive strength is on average 7% higher than the compressive strength in the first series of experiments (Amir et al., 2016; Lantsoght et al., in review), and the tensile strength is on average 12% higher than in the first series. One should consider this difference when comparing the results of the two series of experiments. The measured concrete compressive strength at the age of testing the deck is included in **Table 1** for the static tests and in **Table 2** for the fatigue tests.

The properties of the prestressing steel were not tested again for this series of experiments, as the same prestressing bars from the previous setup were reused. The prestressing bars are Y1100H steel, which has a characteristic tensile strength f_{pk} = 1,100 MPa (160 ksi). The prestressing steel in the prefabricated girders is Y1860S (prestressing strands), which has a characteristic tensile strength f_{pk} = 1,860 MPa (270 ksi).

The properties of samples from the mild steel reinforcement were measured. For the bars with a diameter of 8 mm (0.3 in), the average measured yield strength is f_{ym} = 552 MPa (80 ksi) and the average tensile strength is f_{tm} = 641 MPa (93 ksi). For the 10 mm bars (0.4 in), f_{ym} = 516 MPa (75 ksi) and f_{tm} = 625 MPa (91 ksi), for the 12 mm bars (0.5 in) f_{ym} = 527 MPa (76 ksi) and f_{tm} = 623 MPa (90 ksi), and for the 16 mm bars (0.6 in) f_{ym} = 517 MPa (75 ksi) and f_{tm} = 612 MPa (89 ksi).

Reinforcement

The slab and top flanges have mild steel reinforcement (**Fig. 2**c). Since the top flanges serve as part of the prestressed girders and the slab functions as a deck cast in between the girders, there is no continuity of the reinforcement between the slab and top flanges. The reinforcement of the top flange is designed to resist the bending moments caused by the eccentric loading of the top flange. For the deck slabs, only minimum reinforcement with a diameter of 8 mm (0.32 in) at 200 mm (7.9 in) on center top and bottom in the 1.05 m (3.4 ft) direction (60 bars top and bottom in total per deck) and 8 mm (0.32 in) at 240 mm (9.4 in) on center top and bottom in the 12 m (39 ft) direction (5 bars top and bottom in total per deck) is provided. **Fig. 4** shows the reinforcement of the slab, top flange, and the connection between the top flange and the prefabricated girder.

The cast-in-situ elements (slab and crossbeams) were post-tensioned with unbonded prestressing bars with a center-to-center distance of 400 mm (16 in). The ducts had a diameter of 40 mm (1.6 in). The prestressing of the deck results in a compression of 2.5 MPa (363 psi) in the deck.

Instrumentation

Each prestressing bar is equipped with a load cell (37 in total) to verify if the required force is present in each bar, and thus to check if the required transverse prestressing level of 2.5 MPa (363 psi) is introduced in the slab as well as the correct force in the crossbeams. Six additional load cells measure the support reactions of the simply supported prefabricated girders. A load cell measures the applied load in the jack, and an LVDT measures the stroke of the jack. Three lasers measure the deflections in the prefabricated girders at the same position as the load. Close to the load, two lasers and two LVDTs measure the deflection of the deck slab. Four horizontally placed LVDTs at the bottom of the slab measure the crack width of selected cracks. The full measurement report (Koekkoek and van der Veen, 2017a) of these experiments contains the detailed drawings for each experiment with the positions of the sensors.

Loading procedure

For the static tests, the load is applied with a monotonic loading protocol. Up to a load level of 100 kN (22 kip) the load is applied in steps of 25 kN (6 kip), and for the higher load levels, the load is applied in steps of 50 kN (11 kip). The load is kept constant at each load level to inspect the specimen and mark the cracks, see **Fig. 5**a. The load is applied in a displacement-controlled manner. The size of the loading plate is 115 mm × 150 mm × 20 mm (4.5 in × 5.9 in × 0.8 in), which is a half-scale representation of the wheel print of the super single tire used for checking joints in the Netherlands.

For the dynamic tests, the load cycles between a lower value F_{low} and an upper value F_{up} with $F_{low} = 0.10F_{up}$. The loading frequency is 1 Hz. **Fig. 5**b shows the sine wave that is used to apply the dynamic load. The load is applied in a force-controlled manner. The fatigue tests use

variable amplitude loading, and the number of cycles per load level were determined before the experiments. If failure did not occur after a large number of cycles for the highest planned load level, then the load was increased and the fatigue test was extended until the slab punched. At 1,000 cycles, 10,000 cycles, 100,000 cycles, and multitudes of 500,000 cycles the loading is paused at the maximum load level to measure crack widths and mark the cracks.

EXPERIMENTAL RESULTS

Test results and failure modes

Each experiment has a unique ID, which starts with FAT (fatigue series) and indicates the test number, if the test is static (S) or dynamic (D), and the number of wheel prints (1 or 2). For example, FAT11D2 is the 11^{th} test of the FAT series, and is a dynamic test using a double wheel print. The test series consists of 13 experiments: 3 static tests and 10 fatigue tests. Of these experiments, 9 use a single wheel print and 4 a double wheel print.

Table 1 summarizes the results of the static tests. In this table, P_{max} is the failure load, $f_{cm,cube}$ is the concrete compressive strength at the age of testing the deck, which is shown in the table as well. For all static tests in this series, the failure mode was brittle punching.

Table 2 summarizes the results of the fatigue tests. In this table, F_{up} is the upper level of the sine wave used for the loading as shown in **Fig. 5**b. P_{max} is the failure load in the corresponding static test. N is the number of applied cycles at the given load level F_{up}/P_{max}. The different entries per reported test represent the sequence of the applied load levels. For example, for FAT9D2, first 500,000 cycles at F_{up}/P_{max} = 0.59 were carried out, and then 209,800 cycles at F_{up}/P_{max} = 0.65 were carried out, after which failure occurred. The column "Age" shows the age of the specimen at testing, which is a range for tests that lasted more than a day. The value of $f_{cm,cube}$ is the average cube compressive strength determined at the age of testing the specimen, or the values that correspond with the begin and end age of testing the specimen when the test lasted more than a day.

The corresponding static test for FAT2D1, FAT3D1 and FAT4D1 is FAT1S1 (span 1). The corresponding static test for FAT5D1, FAT6D1, FAT12D1 and FAT13D1 is FAT7S1 (span 2). The corresponding static test for FAT9D2 is FAT8S2 (span 2). For FAT10D2 and FAT11D2, no equivalent static test on span 1 is available, but P_{max} is estimated as follows:

$$\frac{P_{\max,FAT1S1}}{P_{\max,FAT7S1}} \times P_{\max,FAT8S2} = 570.8kN = 128kip$$

The first two fatigue tests, FAT2D1 and FAT3D1 are used to check the difference between the current test setup and the previous test setup (with BB32 as comparable test). Since most of the experiments from the first series of experiments with variable amplitude loading had increasing load levels, the majority of the experiments in the current series have a high load level first (FAT2D1, FAT3D1, FAT5D1, FAT6D1, FAT10D2, FAT11D2). Low to high load levels are only used for FAT4D1 with one wheel load and FAT9D2 with a double wheel print. Experiments FAT12D1 and FAT13D1 use a high value of F_{up}/P_{max} to study low-cycle fatigue. **Fig. 6** gives an overview of the loading positions on the test specimen. The experiments were carried out sequentially, with the date since casting of the deck indicated in **Table 2.**

Resulting *S*-*N* curve

To study the presented fatigue experiments, the *S*-*N* curve is developed, with $S = F_{up}/P_{max}$ the force ratio and *N* the number of cycles to failure. Since the variable amplitude experiments used different levels of loading, the results are analyzed in a conservative way. The loading sequence and number of cycles for FAT2D1 is shown in **Table 2**. FAT2D1 was subjected to 3,285,217 cycles in total: 100,000 cycles between 24 kN and 240 kN (5.4 kip and 54 kip), then 2,915,123 cycles between 20 kN and 200 kN (4.5 kip and 45 kip), then 100,000 cycles between 24 kN and 240 kN (5.4 kip and 54 kip), then 150,000 cycles between 26 kN and 260 kN (5.8 kip and 58 kip), and finally 20,094 cycles between 28 kN and 280 kN (6.3 kip and 63 kip), at which failure occurred. It is thus conservative to assume that the specimen would have at least resisted 3,285,217 cycles between 20

kN and 200 kN (4.5 kip and 45 kip), at least 370,094 cycles between 24 kN and 240 kN (5.4 kip and 54 kip), 170,094 cycles between 26 kN and 260 kN (5.8 kip and 58 kip), and 20,094 cycles between 28 kN and 280 kN (6.3 kip and 63 kip). This approach results in 28 datapoints from the 10 experiments which are used to draw the *S-N* curve, see **Fig. 7**. The expression of the *S-N* diagram (average values) is:

$$S = -0.064 \log N + 1.011 \quad (2)$$

Sequence of load levels

In the first series of experiments, all experiments had an increasing amplitude when a variable amplitude loading was used except for BB32. In the current series, the majority of the experiments had variable amplitude loading for which first a high load level was applied. The results of BB32 seemed to indicate that applying a high load level first reduces the fatigue life. With the results from the current series of experiments, the influence of the sequence of load levels can be studied. For this purpose, the *S-N* diagram with the results from the high-to-low variable amplitude tests is compared to the diagram with the results from the low-to-high tests, see **Fig. 8**. The resulting expression for the low-to-high experiments is:

$$S = -0.062 \log N + 0.950 \quad (3)$$

The expression for the high-to-low experiments is:

$$S = -0.066 \log N + 1.002 \quad (4)$$

As can be seen from these expressions and **Fig. 8**, the influence of the sequence of load levels is negligible. It has thus been shown that there is no reason for concerns (which were raised based on the result of BB32) regarding the influence of the sequence of load levels on the fatigue life. A full description of the analysis of the test results can be found in the analysis report (Koekkoek and van der Veen, 2017b).

Single or double wheel load

Comparing the results of the static experiments can be used to calculate the increased load that can

be applied for a double wheel print as compared to a single wheel print. To calculate this value, the results from FAT7S1 and FAT8S2 can be compared, which gives a ratio of 1.64. Combining this result with the ratio of 1.48 from the BB test series gives an average increase of the maximum load with 1.56 for a double wheel print as compared to a single wheel print.

To check the relation between testing with a single or double wheel load, the *S*-*N* curves of the experiments with a single wheel load and with a double wheel load are represented separately, see **Fig. 9**. **Fig. 7** already indicates that the experimental results for a single and double wheel load follow a similar trend. The resulting *S*-*N* relation for the experiments with a single wheel load is **(Fig. 9**a):

$$S = -0.066 \log N + 1.026 \quad (5)$$

The resulting *S*-*N* for the experiments with a double wheel load is (**Fig. 9**b):

$$S = -0.045 \log N + 0.885 \quad (6)$$

Comparing these expressions and the plots in **Fig. 9** shows that the slope of the experiments with a double wheel print is lower than the slope of the experiments with a single wheel print. The extrapolated value for 1 cycle is lower for the case of a double wheel print than for a single wheel print. However, for the data set of experiments with a double wheel print, no low-cycle fatigue results are available. As such, evaluating the results for a low number of cycles based on the results of the data set of experiments with two wheel prints may not be advisable. For 1 million cycles, *S* according to Eq. (5) is 0.63 and according to Eq. (6) is 0.62. For the range of cycles that have been tested, the differences between a single wheel load and a double wheel load are thus not important for the evaluation of existing slab-between-girder bridges.

Comparison to previous fatigue experiments

The results of the current series of fatigue FAT tests (28 data points) can be compared to the previous BB series (16 data points). The differences between the data sets are the result of the different values of the concrete compressive strength and differences in the test setup. Comparing

Eq. (1) and Eq. (2) shows that the slope of the two expressions is similar, but that the extrapolated value for 1 cycle is higher for the FAT experiments than for the BB experiments. For a general quantification of the effect of fatigue on the punching shear behavior of slab-between-girder bridges, the results from both series can be combined, see **Fig. 10**. The resulting overall *S-N* expression is then:

$$S = -0.062 \log N + 0.969 \quad (7)$$

DISCUSSION

From Eq. (7) follows that for 1 million cycles the maximum load ratio *S* is 60%, for 10 million cycles it is 54% and for 100 million cycles 47%. The resulting fatigue strength resulting from the experiments is similar to fatigue tests of structural concrete and the fatigue resistance of concrete under compression. The experiments from the second series result in a slightly longer fatigue life than from the first series. The difference between the series lies in the tested specimen: for the first series the deck was cast in between the girders, whereas for the second series the deck and the top flange of the prefabricated girders were cast in the laboratory. In the second series, the reinforcement ratio in the deck was higher than in the first series because of the larger diameter of the reinforcement bars.

The specimen that was test during the first and second series of static and fatigue tests had a center-to-center distance between the girders of 1.8 m (5.9 ft), modeled after an existing bridge with a girder spacing of 3.6 m (11.8 ft). This distance is the largest girder spacing for slab-between-girder bridges in the Netherlands, and results in the largest slenderness ratio (15.7) of this subset of bridges. Since for other bridges the spacing is smaller and the resulting slenderness is smaller, it is conservative to extrapolate the results of this most unfavorable case to the rest of the subset of slab-between-girder bridges.

In general, the results indicate that under fatigue loading, compressive membrane action can

still enhance the capacity of slab-between-girder bridges. As such, the enhancement from compressive membrane action can be taken into account for the assessment of slab-between-girder bridges.

SUMMARY AND CONCLUSIONS

For static loading, compressive membrane action enhances the punching shear capacity of slab-between-girder bridges. Previous research studied whether or not compressive membrane action also enhances the capacity of such structures under fatigue loading. From these experiments, some concerns were raised regarding the sequence of loading in variable amplitude fatigue tests, and on the effect of a single wheel print versus a double wheel print.

A half-scale model of a slab-between-girder bridge was built in the laboratory. In this series of experiments, prefabricated inverted T girders were used, and the top flange of the girders as well as the deck slab were cast in the laboratory. This arrangement is different from the first series of experiments for which the full prestressed girder was prefabricated and only the deck slab was cast in between the girders in the laboratory. Comparing the results of the two series of experiments shows that the overall structural behavior of both specimens is comparable and that the resulting datapoints can be studied together.

On the new test setup, 13 experiments were done: 3 static tests and 10 fatigue tests, of which 2 tests with low-cycle fatigue. For 9 experiments a single wheel print was used and for 4 experiments a double wheel print. The failure mode for all experiments was punching shear, as also observed in the first series of experiments and the corresponding static tests that explored the effect of compressive membrane action in slab-between-girder bridges.

The conclusions from these new experiments are that the influence of the sequence of load levels for variable amplitude fatigue tests is not important. The concerns with regard to the effect of cycles with a high level loading before cycles with low level loading are thus not confirmed with

these experiments. For experiments with a double wheel load overall similar behavior was found as for experiments with a single wheel load. The maximum load for the case with a double wheel load is 1.56 times the maximum load for the case with a single wheel load.

The new experiments confirm the first series of experiments. The resulting *S-N* curve that can be used for transversely prestressed decks in slab-between-girder bridges is:

$$S = -0.062 \log N + 0.969$$

Ultimately, these experiments confirm that compressive membrane action enhances the punching capacity of transversely prestressed decks in slab-between-girder bridges, and that the concerns with regard to possible loss of this mechanism are unfounded.

ACKNOWLEDGMENTS

The authors wish to express their gratitude and sincere appreciation to the Dutch Ministry of Infrastructure and the Environment (Rijkswaterstaat) for financing this research work. We are deeply indebted to our colleague Albert Bosman for his work in the laboratory.

NOTATION

$f_{cm,cube}$	average measured cube concrete compressive strengthf
f_{pk}	tensile strength of prestressing steel
$f_{sp,m}$	average measured concrete splitting strength measured on cubes
f_{tm}	tensile strength of reinforcement steel
f_{ym}	yield strength of reinforcement steel
F_{low}	the lower load level in the fatigue tests
F_{up}	the upper load level in the fatigue tests
N	number of cycles
P_{max}	failure load
S	ratio between applied load and failure load

REFERENCES

Amir, S., 2014, "Compressive Membrane Action in Prestressed Concrete Deck Slabs," Ph.D. Thesis, Delft University of Technology, pp. 317.

Amir, S., Van der Veen , C., Walraven, J. C. and de Boer, A., 2016, "Experiments on Punching Shear Behavior of Prestressed Concrete Bridge Decks," *ACI Structural Journal*, V. 113, No. 3, pp. 627-636.

CEN, 2003, "Eurocode 1: Actions on structures - Part 2: Traffic loads on bridges, NEN-EN 1991-2:2003," Comité Européen de Normalisation, Brussels, Belgium, 168 pp.

CEN, 2005, "Eurocode 2: Design of Concrete Structures - Part 1-1 General Rules and Rules for Buildings. NEN-EN 1992-1-1:2005," Comité Européen de Normalisation, Brussels, Belgium, 229 pp.

Chen, Y., Chen, X. and Bu, J., 2018, "Nonlinear damage accumulation of concrete subjected to variable amplitude fatigue loading," *Bulletin of the Polish Academy of Sciences, Technical Sciences*, V. 66, No. 2, pp. 157-163.

El-Bahy, A., Kunnath, S., Stone, W. and Taylor, A., 1999, "Cumulative Seismic Damage of Circular Bridge Columns: Variable Amplitude Tests," *ACI Structural Journal*, V. 96, No. 5, 9/1/1999.

El-Ragaby, A., El-Salakawy, E. and Benmokrane, B., 2007, "Fatigue Life Evaluation of Concrete Bridge Deck Slabs Reinforced with Glass FRP Composite Bars," *Journal of Composites for Construction*, V. 11, No. 3, pp. 258-268.

Ghammouri, M., Abbadi, M., Mendez, J., Belouettar, S. and Zenasni, M., 2011, "An approach in plastic strain-controlled cumulative fatigue damage," *International Journal of Fatigue*, V. 33, No. 2, 2011/02/01/, pp. 265-272.

Ju, M., Oh, H. and Sim, J., 2017, "Indirect fatigue evaluation of CFRP-reinforced bridge deck slabs under variable amplitude cyclic loading," *KSCE Journal of Civil Engineering*, V. 21, No. 5, July 01,

pp. 1783-1792.

Keerthana, K. and Chandra Kishen, J. M., 2018, "An experimental and analytical study on fatigue damage in concrete under variable amplitude loading," *International Journal of Fatigue*, V. 111, 2018/06/01/, pp. 278-288.

Koekkoek, R. T. and van der Veen, C., 2017a, "Measurement Report Fatigue Tests on Slabs Cast In-Between Prestressed Concrete Beams," Stevin Report 25.5-17-14, 196 pp.

Koekkoek, R. T. and van der Veen, C., 2017b, "Analysis of Test Results forFatigue Tests on Slabs Cast In-Between Prestressed Concrete Beams," Stevin Report 25.5-17-15, 21 pp.

Koekkoek, R. T., van der Veen, C. and de Boer, A., 2018, "Fatigue Tests on Post-tensioned Bridge Decks," *Proceedings of the 2017 fib symposium*, pp. 912-920.

Lantsoght, E. O. L., van der Veen, C., de Boer, A. and Walraven, J. C., 2013a, "Recommendations for the Shear Assessment of Reinforced Concrete Slab Bridges from Experiments " *Structural Engineering International*, V. 23, No. 4, pp. 418-426.

Lantsoght, E. O. L., van der Veen, C. and Walraven, J. C., 2013b, "Shear in One-way Slabs under a Concentrated Load close to the support," *ACI Structural Journal*, V. 110, No. 2, pp. 275-284.

Lantsoght, E. O. L., van der Veen, C. and de Boer, A., 2016, "Proposal for the fatigue strength of concrete under cycles of compression," *Construction and Building Materials,* V. 107, No. 15 March 2016, pp. 138-156.

Lantsoght, E. O. L., Van der Veen , C., Koekkoek, R. T. and Sliedrecht, H., in review, "Fatigue testing of transversely prestressed concrete decks," *ACI Structural Journal*.

Regan, P. E. and Braestrup, M. W., 1985, "Punching Shear in Reinforced Concrete," CEB Bulletin 168, 241 pp.

van Leeuwen, J. and Siemes, A. J. M., 1979, "Miner's rule with respect to plain concrete," *Heron*, V. 24, No. 1, pp. 1-34.

Walraven, J. C., 2002, "Background document for EC-2, Chapter 6.4 Punching Shear," Delft

University of Technology, Delft, The Netherlands, 1-16 pp.

TABLES AND FIGURES

List of Tables

Table 1 – Overview of static tests. Conversion: 1 kN = 0.225 kip, 1 MPa = 145 psi

Table 2 – Overview of fatigue tests. Conversion: 1 kN = 0.225 kip, 1 MPa = 145 psi

Table 1 – Overview of static tests. Conversion: 1 kN = 0.225 kip, 1 MPa = 145 psi

Test number	P_{max} (kN)	Age (days)	$f_{cm,cube}$ (MPa)
FAT1S1	347.8	94	82.2
FAT7S1	393.7	240	88.8
FAT8S2	646.1	245	88.6

Table 2 – Overview of fatigue tests. Conversion: 1 kN = 0.225 kip, 1 MPa = 145 psi

Test number	F_{up} **(kN)**	F_{up}/P_{max}	N	**Age (days)**	$f_{cm,cube}$ **(MPa)**
FAT2D1	240	0.69	100,000	102 - 144	82.6 - 84.6
	200	0.58	2,915,123		
	240	0.69	100,000		
	260	0.75	150,000		
	280	0.81	20,094		
FAT3D1	240	0.69	200,000	149 - 168	84.9 – 85.8
	200	0.58	1,000,000		
	240	0.69	100,000		
	260	0.75	300,000		
	280	0.81	6,114		
FAT4D1	200	0.58	1,000,000	169 – 190	85.8 – 86.8
	240	0.69	200,000		
	260	0.75	100,000		
	280	0.81	63,473		
FAT5D1	280	0.71	10,000	192 – 217	91.6 – 89.6
	200	0.51	1,000,000		
	240	0.61	100,000		
	260	0.66	1,000,000		
	280	0.71	1,424		
FAT6D1	280	0.71	10,000	219 – 239	89.6 – 88.8
	200	0.51	1,000,000		
	240	0.61	100,000		
	280	0.71	160,000		
	200	0.51	410,000		
	280	0.71	26,865		
FAT9D2	380	0.59	500,000	246 - 255	88.5 – 88.2

	420	0.65	209,800		
FAT10D2	360	0.63	100,000	260 – 284	90.2 – 91.3
	320	0.56	1,000,000		
	360	0.63	950,928		
FAT11D2	380	0.67	100,000	288 – 315	91.5 – 92.8
	340	0.60	1,000,000		
	380	0.67	1,100,000		
	420	0.75	1,720		
FAT12D1	350	0.89	30	318	85.9
FAT13D1	340	0.86	38	319	85.8

1

2

List of Figures

Fig. 1–Geometry of specimen: (a) top view showing three prestressed girders and two deck panels; (b) side view showing section of the slab-between-girder structural system. All units are mm. Conversion: 1 mm = 0.04 in, 1 m = 3.3 ft.

Fig. 2–Construction of test setup: (a) Prefabricated prestressed girders, with lateral support system; (b) formwork of the slab and top flanges of the girders; (c) reinforcement of the slab and top flanges of the girders; (d) casting of the slab and top flanges of the girders; (e) complete test setup, with loading frame and instrumentation.

Fig. 3–Prefabricated prestressed girder. Dimensions in mm. Conversion: 1 mm = 0.04 in.

Fig. 4–Reinforcement details of slab, top flange, and connection between prefabricated girder and top flange cast in the laboratory. Dimensions in mm. Conversion: 1mm = 0.04 in.

Fig. 5–Loading protocol for fatigue series: (a) static loading; (b) excerpt from dynamic loading.

Fig. 6-Position of experiments and numbering of transverse prestressing bars in the deck slab.

Fig. 7- Resulting *S-N* curve of FAT series of experiments, showing average *S-N* relation as well as 5% lower and 95% upper bound values. 1W is used for experiments with a single wheel print and 2W for the experiments with a double wheel print.

Fig. 8-Influence of loading sequence on *S-N* curve.

Fig. 9-Influence of type on loading on *S-N* curve: (a) single wheel print results; (b) double wheel print results.

Fig. 10-Resulting *S-N* curve from the combination of BB and FAT fatigue experiments.

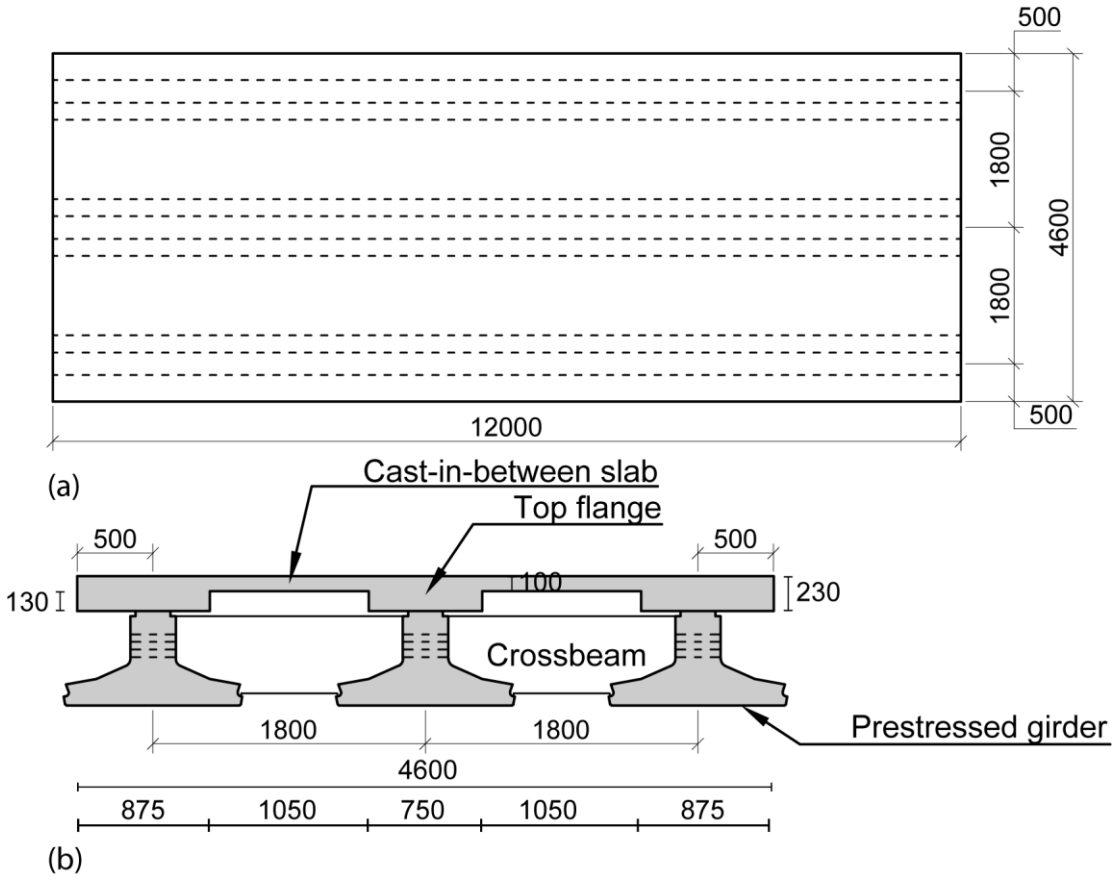

Fig. 1–Geometry of specimen: (a) top view showing three prestressed girders and two deck panels; (b) side view showing section of the slab-between-girder structural system. All units are mm. Conversion: 1 mm = 0.04 in, 1 m = 3.3 ft.

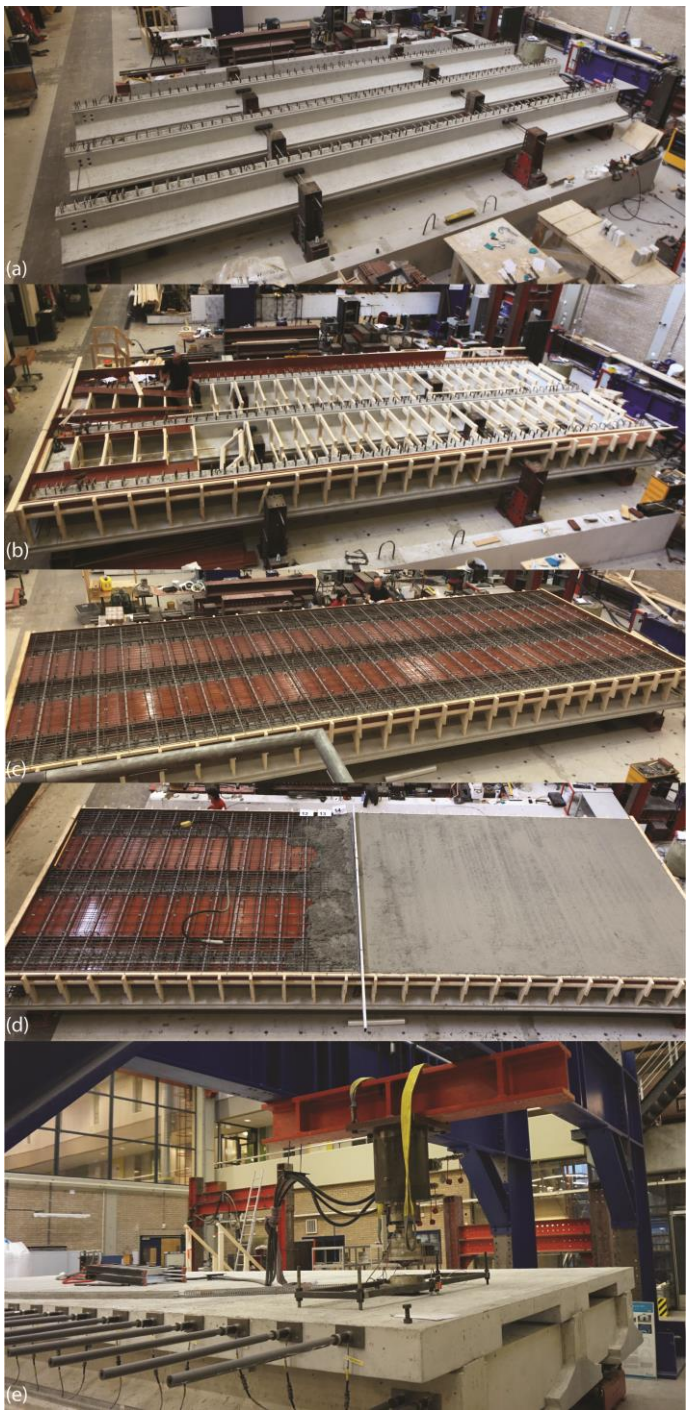

Fig. 2–Construction of test setup: (a) Prefabricated prestressed girders, with lateral support system; (b) formwork of the slab and top flanges of the girders; (c) reinforcement of the slab and top flanges of the girders; (d) casting of the slab and top flanges of the girders; (e) complete test setup, with loading frame and instrumentation.

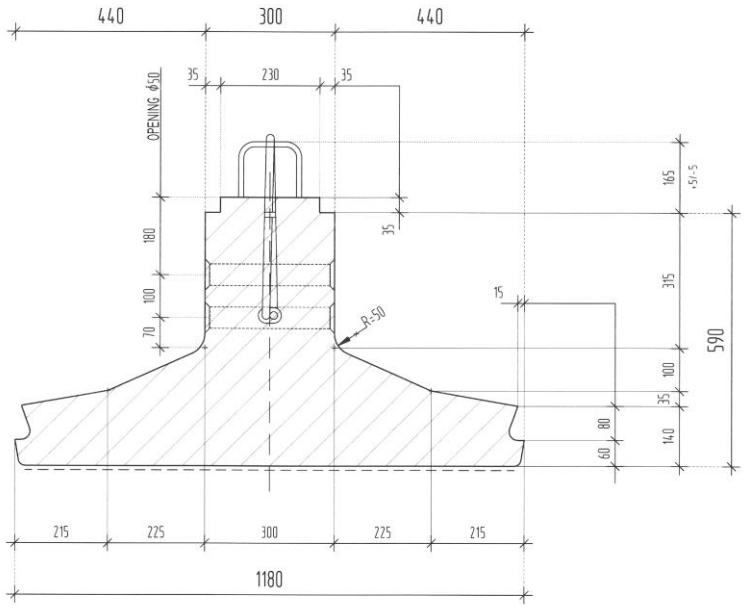

Fig. 3–Prefabricated prestressed girder. Dimensions in mm. Conversion: 1 mm = 0.04 in.

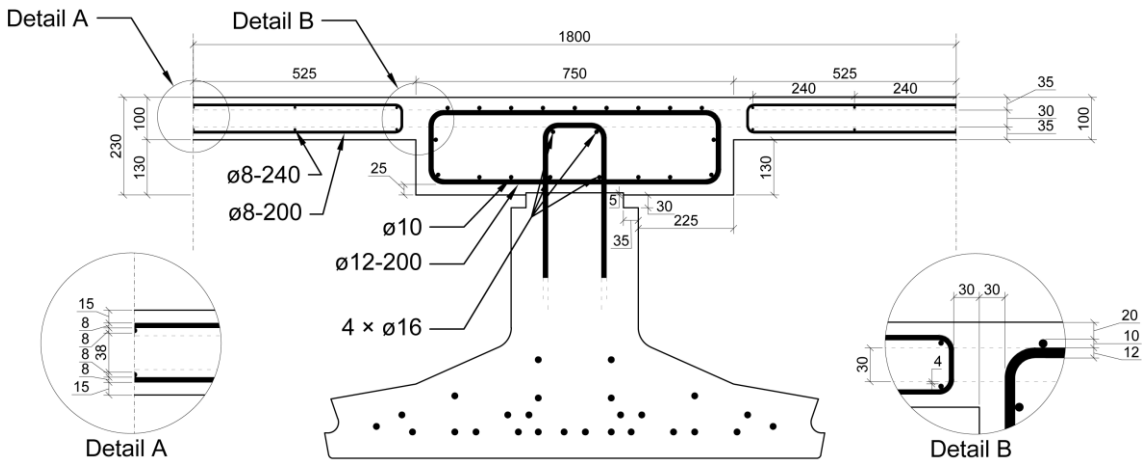

Fig. 4–Reinforcement details of slab, top flange, and connection between prefabricated girder and top flange cast in the laboratory. Dimensions in mm. Conversion: 1mm = 0.04 in.

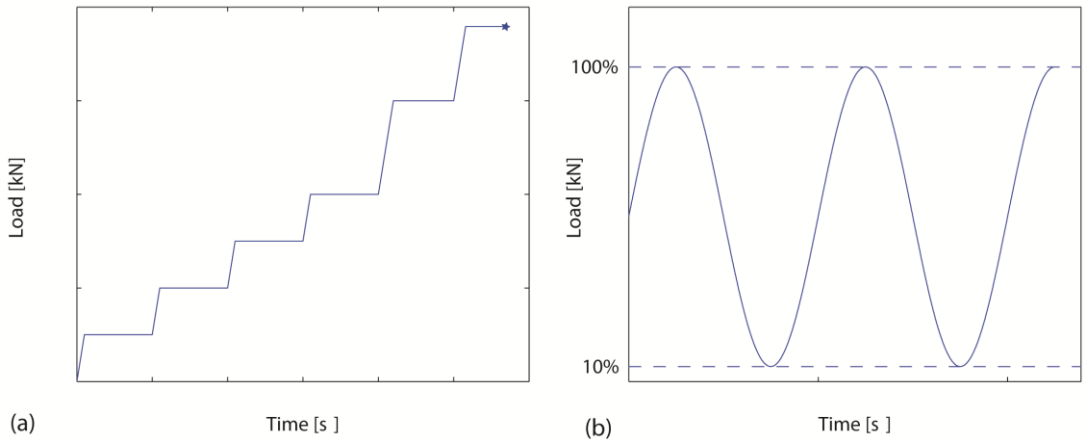

Fig. 5–Loading protocol for fatigue series: (a) static loading; (b) excerpt from dynamic loading.

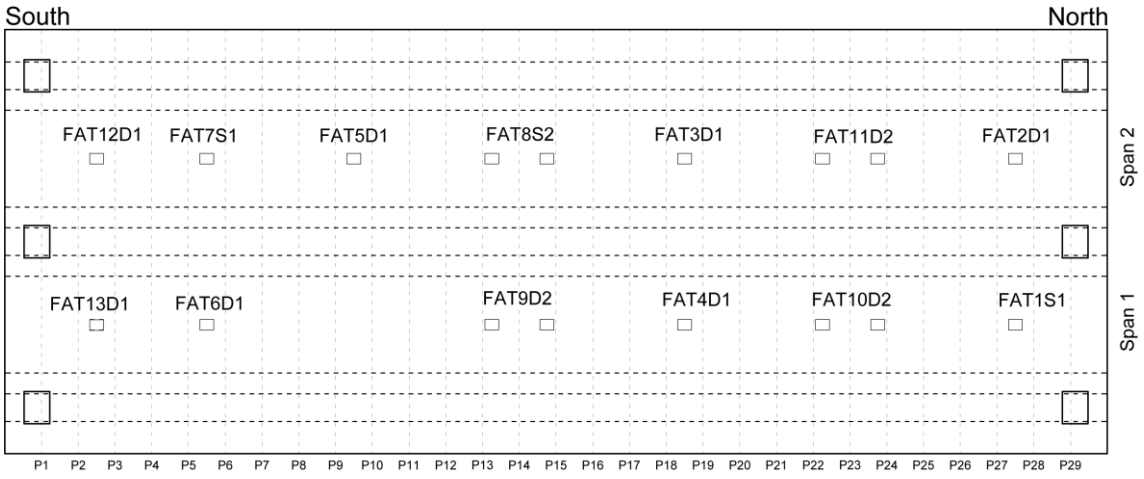

Fig. 6-Position of experiments and numbering of transverse prestressing bars in the deck slab.

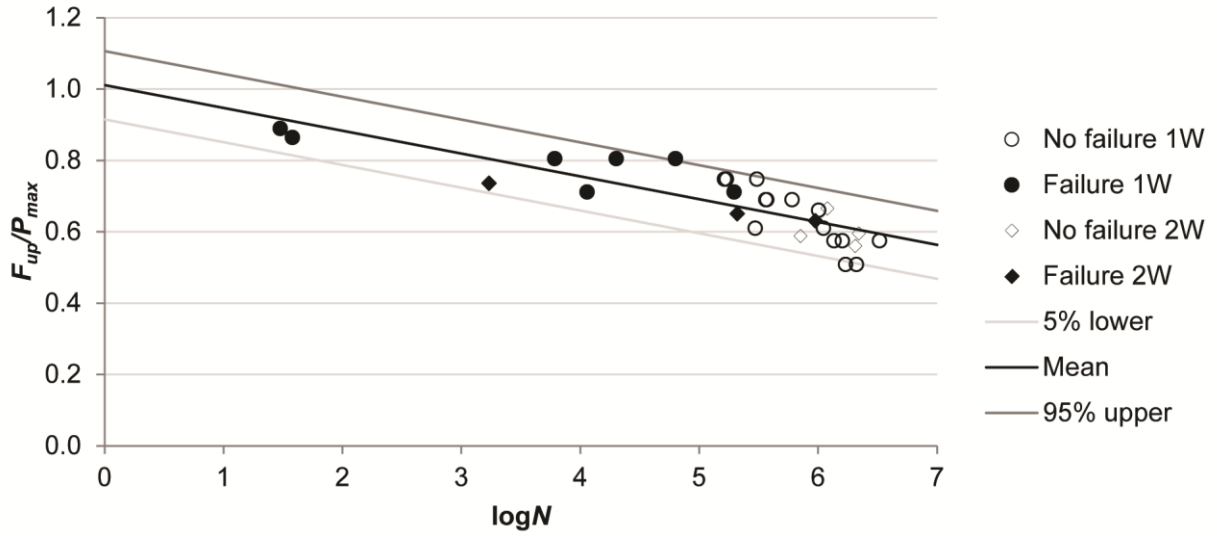

Fig. 7- Resulting *S-N* curve of FAT series of experiments, showing average *S-N* relation as well as 5% lower and 95% upper bound values. 1W is used for experiments with a single wheel print and 2W for the experiments with a double wheel print.

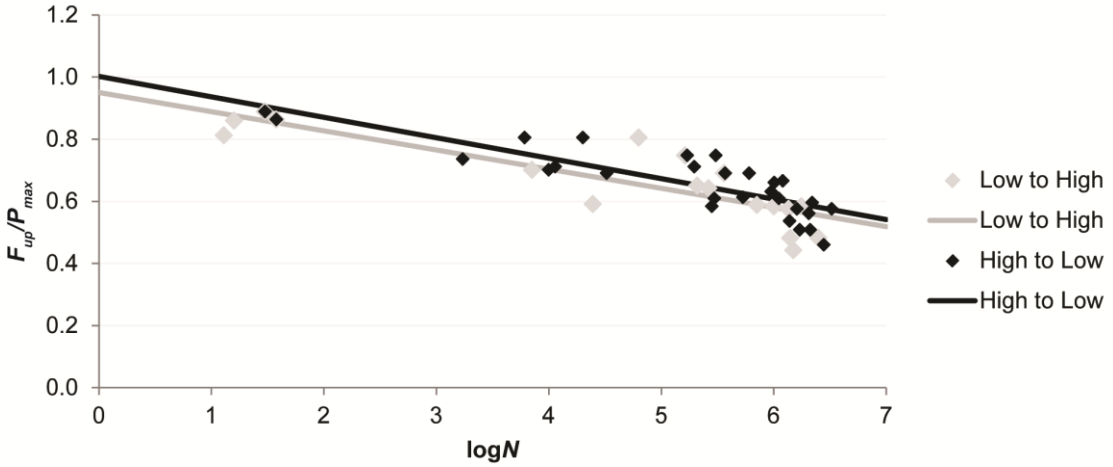

Fig. 8-Influence of loading sequence on *S-N* curve.

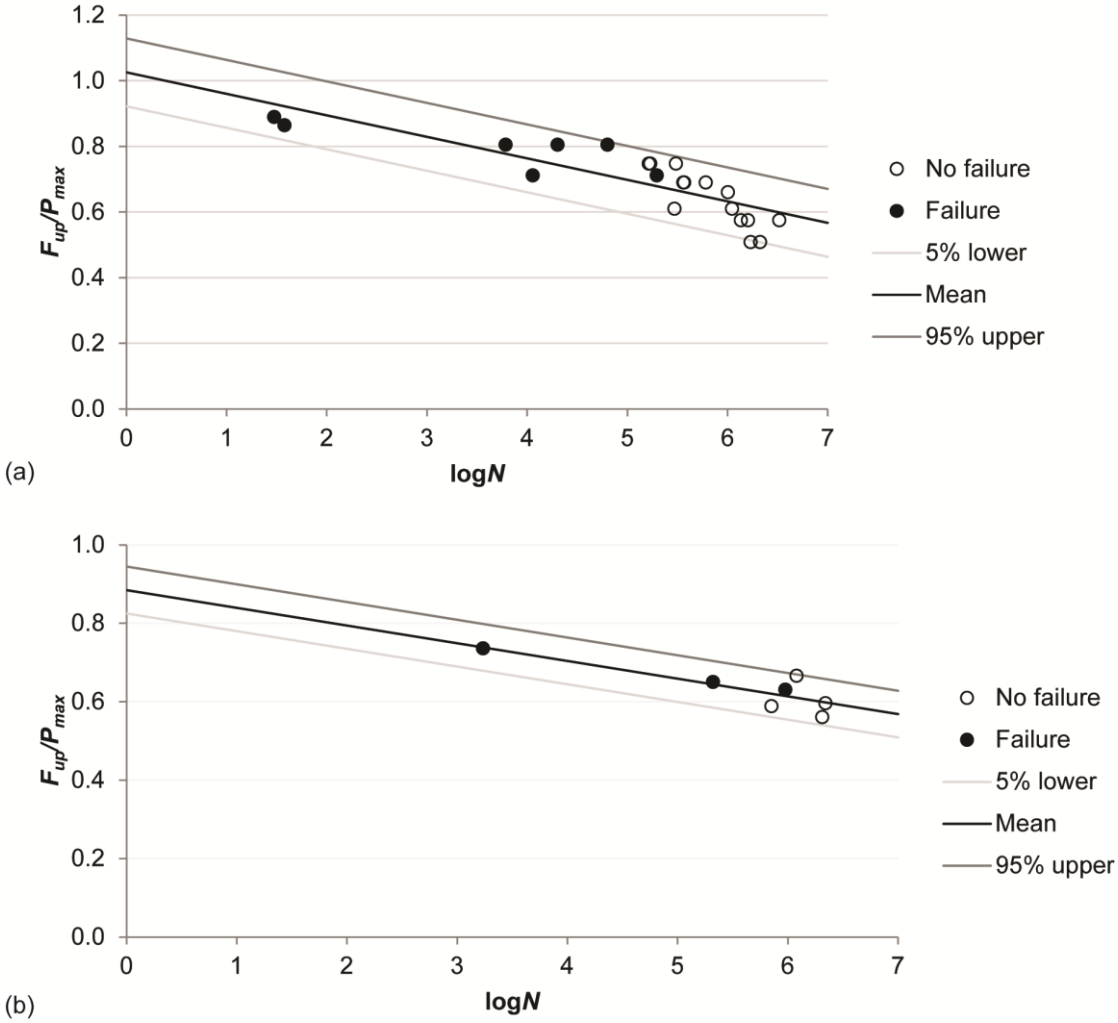

Fig. 9-Influence of type on loading on *S*-*N* curve: (a) single wheel print results; (b) double wheel print results.

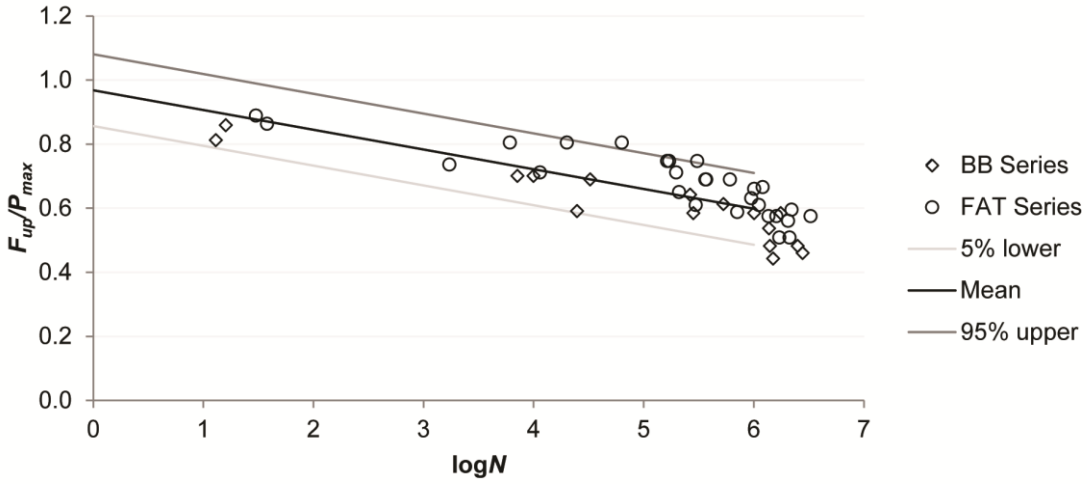

Fig. 10-Resulting *S*-*N* curve from the combination of BB and FAT fatigue experiments.